



## Measurement of substrate thermal resistance using DNA denaturation temperature

David J. Kinahan<sup>a,\*</sup>, Tara M. Dalton<sup>a,b</sup>, Mark R. Davies<sup>a,b</sup>

<sup>a</sup> Stokes Bio Ltd, Shannon Arms, Henry Street, Limerick, Republic of Ireland

<sup>b</sup> Dept. Mechanical and Aeronautical Eng., University of Limerick, Limerick, Republic of Ireland

### ARTICLE INFO

#### Article history:

Received 2 November 2008

Received in revised form

30 July 2009

Accepted 30 July 2009

Available online 27 August 2009

#### Keywords:

PCR

Fluorescent melting curve analysis

Denaturation of DNA

Genetic analysis

Thermal resistance

Microchannel

Substrate

### ABSTRACT

Heat Transfer and Thermal Management have become important aspects of the developing field of  $\mu$ TAS systems particularly in the application of the  $\mu$ TAS philosophy to thermally driven analysis techniques such as PCR. Due to the development of flowing PCR thermocyclers in the field of  $\mu$ TAS, the authors have previously developed a melting curve analysis technique that is compatible with these flowing PCR thermocyclers. In this approach a linear temperature gradient is induced along a sample carrying microchannel. Any flow passing through the microchannel is subject to linear heating. Fluorescent monitoring of DNA in the flow results in the generation of DNA melting curve plots. This work presents an experimental technique where DNA melting curve analysis is used to measure the thermal resistance of micro-channel substrates. DNA in solution is tested at a number of different ramp rates and the different apparent denaturation temperatures measured are used to infer the thermal resistance of the micro-channel substrates. The apparent variation in denaturation temperature is found to be linearly proportional to flow ramp rate. Providing knowledge of the microchannel diameter and a non-varying cross-section in the direction of heat flux the thermal resistance measurement technique is independent of knowledge of substrate dimensions, contact surface quality and substrate composition/material properties. In this approach to microchannel DNA melting curve analysis the difference between the measured and actual denaturation temperatures is proportional to the substrate thermal resistance and the ramp rate seen by the sample. Therefore quantitative knowledge of the substrate thermal resistance is required when using this technique to measure accurately DNA denaturation temperature.

© 2009 Elsevier Masson SAS. All rights reserved.

### 1. Introduction

Fluorescent Melting Curve Analysis (FMCA) is a technique through which non-specific fluorescent DNA dyes can be used to recognise an individual DNA product [1]. The thermodynamic stability of double helix DNA (dsDNA) is contingent on both its length and its base pair composition [2,3]; samples of differing length and compositions may be recognised by their differing denaturation temperatures,  $t_m$ . FMCA uses the characteristic variations in sample fluorescence with temperature to identify the denaturation temperature of samples. With increasing temperature the fluorescence of dsDNA in the presence of a dsDNA dye will decrease linearly. However at higher temperatures on the PCR thermocycle — typically between 85 °C and 95 °C — the dsDNA denatures and a non-linear decrease in fluorescence will be observed. The measurement of the temperature at which this non-

linear change in fluorescence occurs permits measurement of the denaturation temperature of PCR product.

FMCA has become an almost ubiquitous feature of quantitative PCR thermocyclers [4]. It is most commonly used as a closed tube technique to ensure the specificity and quality of the PCR sample amplified. The melting curve method can also be used to detect single nucleotide polymorphisms (SNPs) [5] and mutations associated with genetic diseases such as cancer [6]. When combined with appropriate primer/probe selection melting curve analysis becomes an important tool in multiplex PCR [7].

Since the Micro Total Analysis System ( $\mu$ TAS) concept was first proposed [8] a number of technologies have undergone miniaturisation from desktop to 'lab on a chip'. Among these technologies have been the thermocyclers associated with the PCR process. Research on well-based PCR thermocyclers has focused on reducing reaction size [9]. Space-domain (flowing) PCR — where the reaction is moved between zones of fixed temperature [10,11] — has been of interest to many research groups due to its potential for rapid thermocycling, small reaction volumes and high-throughput processing.

\* Corresponding author. Tel.: +353 61446300.

E-mail address: [david.kinahan@stokesbio.ie](mailto:david.kinahan@stokesbio.ie) (D.J. Kinahan).

Progress towards developing FMCA for use with flowing thermocyclers is ongoing [12]. The application of spatial temperature gradients across micro-fluidic substrates has been previously used for DNA melting analysis in microchannel systems [13–17]. Spatial temperature gradients have also been used to acquire DNA melting curves under non-equilibrium conditions [18]. Denaturation temperature measurements made from surface bound DNA have previously been used to characterise micro-fluidic substrates [19].

The use of low conductivity materials in the manufacture of micro-channel substrates is considered an advantage for many applications [20]. For lab-on-chip space-domain PCR fluidic length scales are small which results in rapid fluid temperature transition between thermal zones [21]. Thermal gradients are present within the substrates during these transitions but are negligible within the thermal zones themselves. However, in order to integrate melting curve analysis in space-domain thermocyclers the fluid must be subject to a steady heat flux through the substrate walls. Thermal gradients will be present through the substrate at all points of the melting curve analysis resulting in an apparent temperature difference between melting curves measured in a microchannel compared with those measured in a reference platform. In this approach knowledge of substrate thermal resistance is important as the magnitude of the apparent temperature discrepancy is proportional to the substrate thermal resistance. Much work has been done towards characterising heat transfer in microchannels [22,23] particularly for applications in electronic cooling although thermal characterisation of micro-fluidic substrates for applications in biomedical research has become increasingly important [24–26].

In this paper melting curve analysis is performed by pumping DNA in solution along a microfluidic channel. The test platform consists of two thermal blocks which sandwich a microfluidic channel. This channel is transparent Teflon FEP tubing with an internal diameter of 400  $\mu\text{m}$ . During experimental testing the channel is aligned within the test platform using two different substrates. Substrate A is composed of polycarbonate while Substrate B is composed of a polycarbonate base with a glass cover-sheet. DNA melting curves are measured in each substrate using a variety of flow velocities and the effects are recorded. These findings are supported using a simple heat transfer analysis. Results are then substituted into the theoretical treatment to infer the thermal resistance between the thermal blocks and the fluid flow within the microchannels. With the caveats that the microchannel be of known uniform cross-section and that the composition of the substrate be homogenous in the direction of heat flux; this technique can measure the thermal resistance irrespective of knowledge of substrate dimensions, contact surface quality or substrate composition/material properties.

## 2. Experimental design and methods

The test device consists of two aluminium blocks of length 120 mm, width 50 mm and minimum thickness 10 mm. These thermal blocks are designed to sandwich a substrate which either has a microfluidic channel directly etched into it or — as in the case described here — aligns and secures disposable tubing within the test rig. Thick film heaters and Darlington transistors are attached to one end of the blocks for heating. The opposite end of the block has channels machined to provide for liquid cooling via a precision thermal bath. As illustrated in Fig. 1(a), a slot of dimensions 84 mm long and 2 mm wide is machined into the upper block to provide optical access to the substrate. Four thermocouples are embedded in the lower thermal block such that they align with the optical access groove when the blocks are mated. The sample is pumped through transparent, disposable Teflon FEP tubing (Upchurch Scientific). This tubing has an outer diameter of approximately

800  $\mu\text{m}$  and inner diameter of approximately 400  $\mu\text{m}$ . Two different substrates are used to align the Teflon FEP tubing within the device.

Substrate A is manufactured from a 1 mm thick transparent polycarbonate sheeting. This is cut to 120 mm  $\times$  50 mm, the footprint of the test rig thermal blocks, and is assembled as shown in Fig. 1(c). The two lower ply are sprayed black and are glued together. The cover-sheet ply is transparent and is held in place when the blocks are assembled. Substrate B, shown in Fig. 1(d), consists of a similar polycarbonate base plate of near identical dimensions but is fitted with a cover-sheet manufactured from borosilicate glass. This cover-plate is composed of two microscope 1 mm thick, 26 mm wide and 80 mm long. One slide is located directly over the point in the optical access groove where DNA denaturation is expected to occur. The second slide is located upstream. Due to the orientation of the excitation laser, at the point where the two microscope slides meet total internal reflection results in some component of laser illumination being reflected directly at the emission sensor, causing noise. Additionally, this total internal reflection also shadows part of the channel from excitation light resulting in a drop in fluorescent signal in this part of the optical access groove. The effects of this may be seen at  $\approx 80^\circ\text{C}$  upon the melt curves presented in Fig. 2, where following moving average smoothing it appears as a wavelike ripple. As this effect occurs away from the denaturation section of the melting curves it has no effect upon the denaturation temperatures measured.

Samples are loaded into the Teflon FEP tubing via aspiration and are buffered by an immiscible fluid (M5904 Mineral Oil – Sigma–Aldrich). Samples are slugs approximately 100 mm long, which is greater than the interrogation length (length of optical window) of the device. As the recirculation length for the sample [27] is significantly greater than the interrogation length it is assumed that multiphase effects are trivial and the flow approximates single-phase Hagen–Poiseuille flow. The sample is pumped into the device until it is observed entering the interrogation area and a fluorescent signal is acquired.

Fluorescent illumination was provided using a 488 nm blue laser (BlueSkyResearch). The laser beam was passed through a concave lens (Edmundoptics) to expand and diffuse the excitation beam. Emissions were filtered via a 515 nm long pass filter (Melles–Griot) and the emission sensor was a monochrome CCD camera (The Imaging Source). Fluorescent emissions are proportional to the intensity of excitation light [28]. In order to ensure uniform illumination of the interrogation area throughout individual experiments the heating blocks are mounted on a positioning stage. As the sample flows down the microfluidic channel at a given velocity the test device is moved at a velocity of identical magnitude but opposite direction. The sample therefore remains within the interrogation area and stationary relative to the excitation light source and emission sensor. Sample pumping is via a syringe pump (Harvard Apparatus PHD2000). The experimental setup is illustrated in Fig. 1(b).

On activation of data acquisition the appropriate flow rates and slew rates are calculated automatically (based on the ramp rate selected by the user) for the syringe pump and positioning stage respectively. In some cases the sample was aspirated back through the device and then retested. The experimental conditions used during testing are outlined in Table 1. For convenience the spatial temperature gradient applied across the blocks will be referred to in terms of the temperature difference between both ends of the optical access groove,  $\Delta T_{\text{OAG}}$ . This experimental rig was previously characterised using substrates of a similar composition but larger internal diameter [29] using in-channel thermocouple measurements. Temperature measurements were made at 0.1 mm intervals

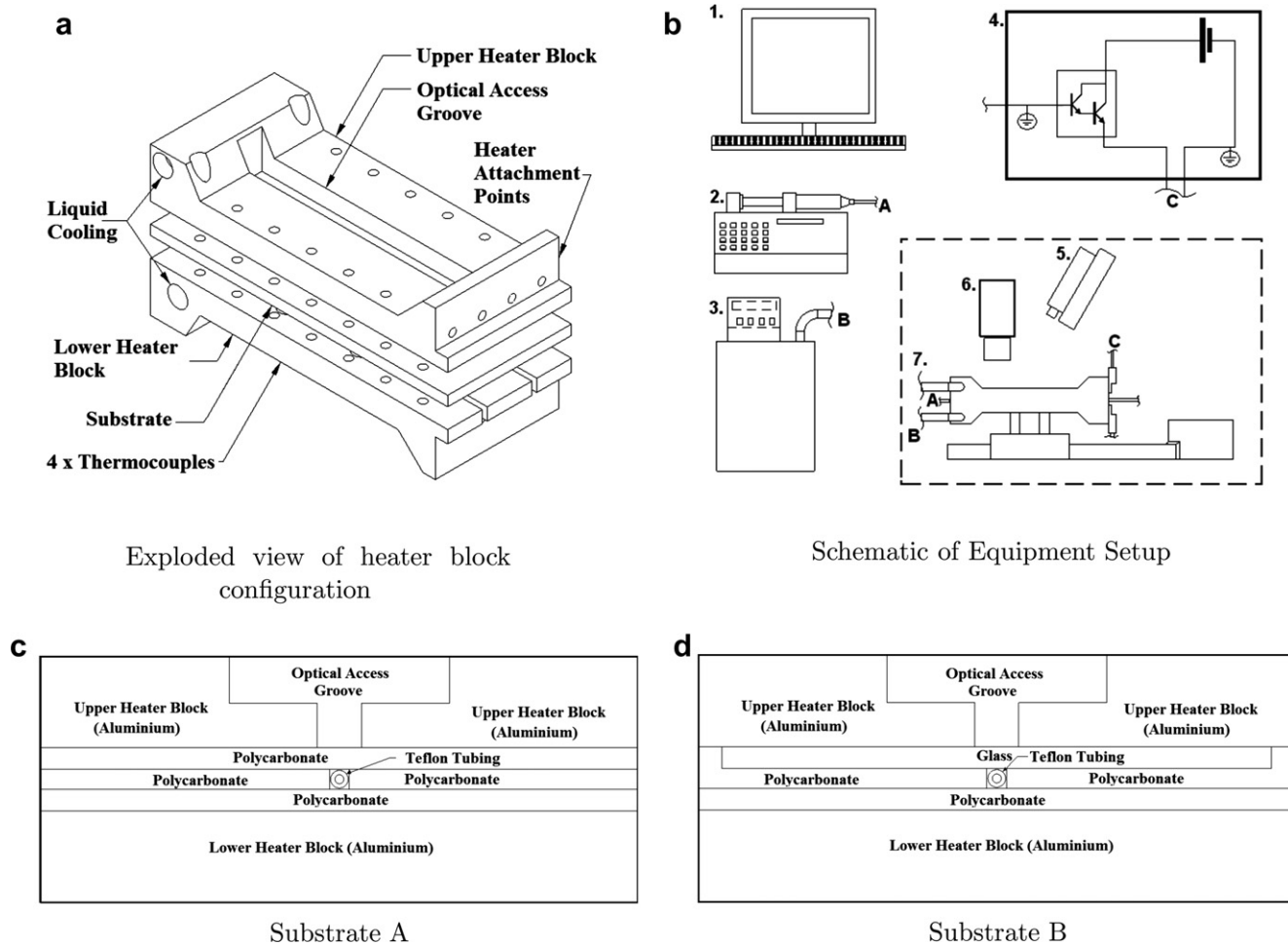


**Fig. 1.** Equipment setup and Substrate compositions. Fig 1(b) shows 1. Computer for control/datalogging. 2. Syringe Pump. 3. Heater bath for cooling. 4. Control circuit for heaters. 5. Excitation Laser. 6. Monochrome Camera. 7. Thermal Blocks mounted on Positioning Stage. A–A, B–B and C–C indicate connection of sample fluid, cooling fluid and electronic wiring respectively.

using a positioning stage with the position of the thermocouple bead being confirmed using a CCD camera. A line of best fit passed through the temperature field for the optical access groove for the worst performing substrate — manufactured completely from polycarbonate — resulted in a coefficient of determination of  $R^2 = 0.995$ . The temperatures measured by the thermocouples at each end of the optical access groove typically varied by less than  $0.2^\circ\text{C}$  during the course of an experiment.

The denaturation temperature,  $t_m$ , for each DNA melting curve was identified by applying the analysis technique previously described [17].

### 3. Biological material

Two PCR plasmid fragments were amplified from *Escherichia coli* plasmid vector pGEM-5Zf(+) (Promega). A 240 bp plasmid fragment was amplified using a forward primer of sequence 5'-AGG GTT TTC CCA GTC ACG ACG TT-3' and a reverse primer 5'-CAG GAA ACA GCT ATG ACC-3'. A 232 bp plasmid fragment was amplified using forward primer 5'-ATA CCT GTC CGC CTT TCT CC-3' and reverse primer 5'-CCT CGC TCT GCT AAT CCT GT-3'. Primers were acquired from MWG Biotech (Ebersberg, Germany). Fragments were amplified using LightCycler Faststart DNA Master SYBR Green I reaction mix (Roche). Fragments were thermocycled and a melting curve analysis

performed using the Applied Biosystems AB7900 thermocycler; fragments were then frozen at  $-20^\circ\text{C}$  prior to use.

### 4. Theoretical treatment

During experimental testing a temperature field is applied to the upper and lower surfaces of the substrates using thermal blocks. Heater elements and fluidic cooling are used to maintain the temperatures of the end-points of these blocks. Assuming simple 1D conduction heat transfer this temperature field is a linear thermal gradient in the direction of heat flux. The microfluidic channel is on the same axis as heat flux through the thermal blocks. Due to the thermal resistances of both the working fluid and the tubing/substrate walls a temperature difference will exist between the mean temperature of the working fluid and the temperature at the outer surface of the polycarbonate substrate.

As a simplification the experimental platform is treated as cylindrical tube of uniform cross-section with a linear temperature gradient applied along the outer wall. In this configuration single-phase fluid flowing through the channel is subject to a uniform wall heat flux. Therefore the fluid is subject to heating at a constant ramp rate.

The heat energy required to increase the internal energy of the fluid by the appropriate ramp rate [30] is:

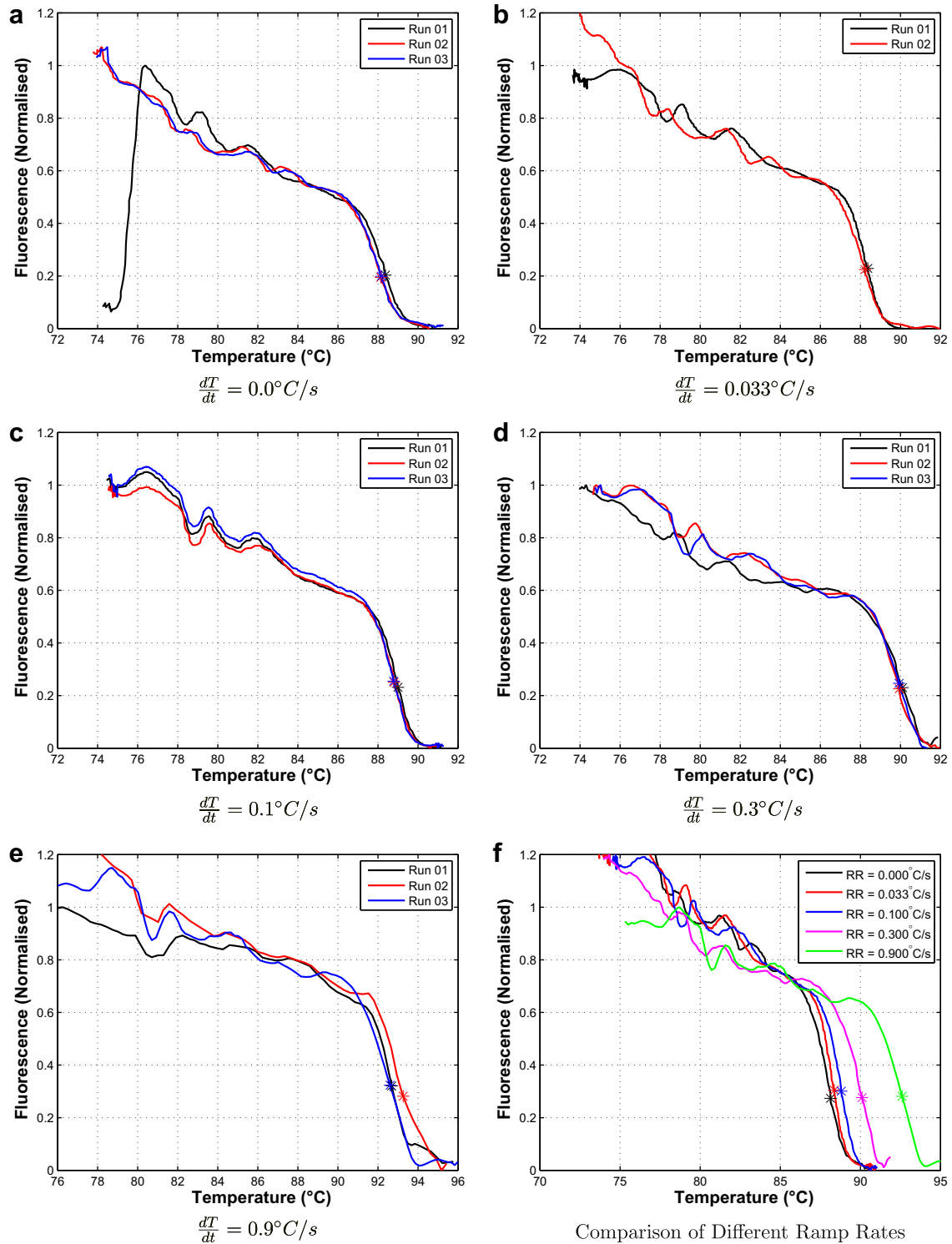


Fig. 2. Plasmid Fragment B (232 bp) Melting Curves measured across a temperature difference of  $\Delta T = 24.0^\circ\text{C}$  using Substrate B.

$$q_w = -c_w \rho_w V_w \frac{dT}{dt} \quad (1)$$

where the fluid is subjected to ramp rate  $dT/dt$ .  $c$  refers to the specific heat capacity of the fluid,  $\rho$  its density and  $V$  is the volume of the fluid.

The ramp rate seen by the fluid is a function of the spatial thermal gradient and the velocity of the fluid through the test rig:

$$\frac{dT}{dt} = \frac{dT}{dx} \frac{dx}{dt} \quad (2)$$

From Equation (1) the heat energy  $q_w$  must enter the fluid element of volume  $V_w$  to increase the temperature of the fluid at

**Table 1**  
Experimental test conditions.

Ramp rate °C/s	Temp. diff. °C	Thermal grad. °C/mm	Velocity mm/s
0.000	24	0.286	0.000
0.033	24	0.286	0.116
0.033	8	0.095	0.350
0.100	24	0.286	0.350
0.100	8	0.095	1.050
0.300	24	0.286	1.050
0.300	8	0.095	3.150

a ramp rate of  $dT/dt$ . In order to enter the fluid heat energy equal to  $q_w$  must pass through the walls of the tubing. This heat transfer must be driven by a temperature difference between the inner and outer walls of the tubing. The magnitude of this heat transfer is

$$q_T = -\frac{k_T A}{x_T} (\Delta T_T) \quad (3)$$

where  $x_T$  is the thickness of the material through which the heat is passing. Equating Equations (1) and (3), re-writing in cylindrical coordinates of infinitesimal axial dimension  $dy$ , and rearranging for the temperature difference through the tubing walls  $\Delta T_T$ :

$$\Delta T_T = -\left(\frac{dT}{dt}\right) \left(\frac{x_T}{k_T(2\pi R\delta y)}\right) (c_w \rho_w \pi R^2 \delta y) \quad (4)$$

From Bejan [31], Equation (5) presents the temperature variation across the fluid within the microchannel,  $\Delta T_F(r)$ , from the wall temperature based upon the application of a uniform wall heat flux to the walls of the fluid element

$$\Delta T_F(r) = -\frac{dT}{dt} \left(1 + 0.5 \left(1 - \frac{r^2}{R^2}\right)\right) \frac{(R^2 - r^2)}{4\alpha_w} \quad (5)$$

where  $r$  the position on the radial axis measured from the centreline,  $R$  the radius of the circular microchannel and  $\alpha$  the thermal diffusivity of the working fluid  $k_w/\rho_w c_w$ .

Assuming constant material properties, dimensions and ramp rate  $dT/dt$ , Equation (4) states a constant temperature difference,  $\Delta T_T$ , will exist between the inner and outer walls of the substrate. It is assumed that a negligible thermal gradient exists across the thermal blocks due to their much greater thermal conductivity. In addition, applying typical values of water as the working fluid and applying them to Equation (5) for the maximum ramp rate used in this project,  $dT/dt = 0.9^\circ\text{C}$ , results in a temperature variation at the microchannel centerline,  $\Delta T_F(0)$ , of less than 0.1 K. Therefore only the temperature variation through the substrates,  $\Delta T_T$ , will be considered.

From Equation (4), the temperature difference across the microchannel walls,  $\Delta T_T$ , is a function of the ramp rate seen by the fluid, ( $dT/dt$ ), the thermal resistance of the microchannel walls, ( $x_T/k_T(2\pi R\delta y)$ ), and the thermal capacitance of the fluid, ( $c_w \rho_w \pi R^2 \delta y$ ). Assuming that the thermal properties of the fluid, the cross-section of the microchannel and the thermal resistance of the microchannel walls remain constant; the temperature difference across the tubing walls,  $\Delta T_T$ , will be proportional to the ramp rate seen by the fluid,  $dT/dt$ .

By making measurements at different ramp rates,  $dT/dt$ , it is possible to generate a linear relationship between temperature difference and ramp rate,  $\Delta T_T$  vs  $dT/dt$ . Rearranging Equation (4) this relationship can be used to measure the thermal resistance of the tubing

$$\left(\frac{x_T}{k_T(2\pi R\delta y)}\right) = -\frac{\Delta T_T}{\left(\frac{dT}{dt}\right) (c_w \rho_w \pi R^2 \delta y)} = -\frac{\text{slope of line}}{(c_w \rho_w \pi R^2 \delta y)} \quad (6)$$

This equation is applied to experimental results in order to measure the thermal resistance of a substrate. Assuming the thermal resistance is non-variant in the direction of fluid flow the equation requires no information regarding the physical composition of the tubing, its dimensions or its thermal properties.

## 5. Results

The experimental test conditions applied are outlined in Table 1. These were selected to investigate the effect of varying the flow velocity, varying the spatial temperature gradient and varying the test ramp rates during the course of experimental testing. With  $\Delta T_{OAG} = 24.0^\circ\text{C}$ , measurements at  $dT/dt = 0.0^\circ\text{C/s}$  and  $dT/dt = 0.1^\circ\text{C/s}$  typically resulted in  $\approx 900$  fluorescent measurements being made during the traverse of the DNA sample across the optical access window. For the case of  $dT/dt = 0.033^\circ\text{C/s} \approx 2700$  measurements are made; for  $dT/dt = 0.3^\circ\text{C/s} \approx 300$  measurements are made and for  $dT/dt = 0.9^\circ\text{C/s} \approx 100$  measurements are made. For experiments conducted with a temperature difference of  $\Delta T_{OAG} = 8.0^\circ\text{C}$  the number of measurements for a given ramp rate are typically reduced by a factor of 3 as these tests occur at higher velocities.

Fig. 2 shows melting curves acquired from the 232 bp plasmid fragment. These measurements was made by applying a temperature difference  $\Delta T_{OAG} = 24^\circ\text{C}$  to the outer walls of Substrate B. In this case the DNA sample was recycled through the test rig and retested under the same operating conditions. The melting profiles measured show good repeatability. A variation of less than  $0.3^\circ\text{C}$  in measured denaturation temperature is observed except in the case of  $dT/dt = 0.9^\circ\text{C/s}$  ( $\Delta T_m = 0.6^\circ\text{C}$  (Fig. 2(e))). This increased variation is a function of both the higher velocity at which the sample is tested and the lower resolution of melting profiles acquired at higher ramp rates.

For melting profiles acquired at  $dT/dt = 0.0^\circ\text{C/s}$  the DNA slug was positioned such that it filled the optical access groove. The fluorescent acquisition system then traversed the stationary DNA sample to generate melting curves (Fig. 2(a)). The sharp transition observed at  $75^\circ\text{C}$  in Fig. 2(a) is a result of the transition from measurement of oil to measurement of DNA sample. As described previously the ripples which may be seen in the linear portion of the melting profiles — typically between  $78^\circ\text{C}$  and  $82^\circ\text{C}$  in every plot — are a result of an optical discrepancy in the glass cover-sheet used with Substrate B. Fig. 2(f) presents a comparison of typical melting profiles acquired at different ramp rates. It is clear that increasing the ramp rate at which the melting profiles are acquired has the effect of offsetting apparent denaturation temperature to a higher temperature. As described previously in the theoretical treatment this effect is a function of both the thermal resistance and the ramp rate seen by the fluid. Fig. 3 presents data acquired from a number of different experiments at test conditions outlined in Table 1. Each dataset is normalised by subtracting the mean denaturation temperature measured at  $dT/dt = 0.0^\circ\text{C/s}$  from each measured denaturation temperature. Plotting the temperature difference measured against the ramp rate confirms the linear relationship expected from the theoretical treatment.

Fig. 3 also shows that this trend is independent of DNA fragment used. Under the same test conditions, both the 232 bp and 240 bp plasmid fragments are subject to near identical changes in apparent denaturation temperature. In addition, melting profiles measured at identical ramp rates but different operating conditions show similar apparent denaturation temperatures. Finally, it is clear that varying the composition of the alignment substrate results in a different magnitude of temperature variation. This is a result of the higher thermal conductivity of borosilicate glass — the cover-sheet used in Substrate B — compared with polycarbonate used in

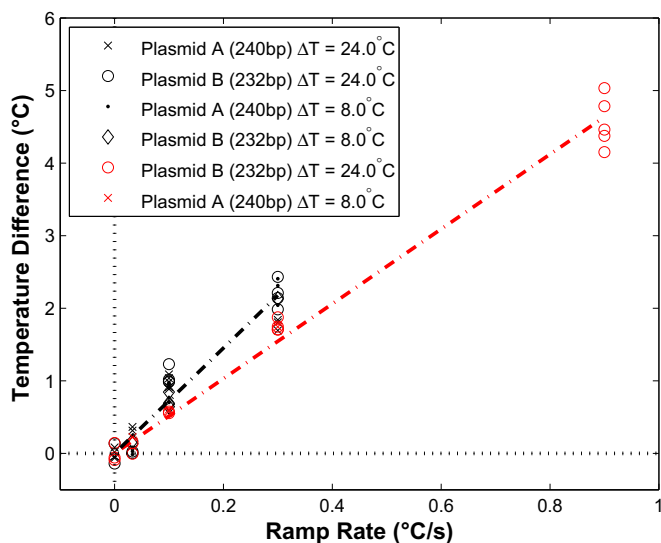


**Fig. 3.** Comparison of the Change in Apparent Denaturation Temperature,  $t_m$ , with respect to ramp rate between measurements made in Substrate A and Substrate B. Measurements from Substrate A are shown in black, while those from Substrate B are shown in red.

the cover-sheet of Substrate A. Under the test conditions applied no useable results were acquired from  $dT/dt = 0.9^\circ\text{C/s}$  in Substrate A as the DNA samples were not fully denatured when leaving the optical access window. Some of the melting curves used to generate the denaturation temperature data shown in Fig. 3 for Substrate A have previously been published [17].

Substituting the slopes of the lines of best fit shown in Fig. 3 into Equation (6) permits estimates of the substrate thermal resistances to be made. These results are presented in Table 2.

## 6. Discussion and conclusions

Thick walled, low conductivity plastic tubing has been used with success in flowing PCR thermocyclers [32,33]. In the PCR case the flow transitions between two or three isothermal zones. Past the entry length the heat flux required to maintain fluid temperature is minimal. Hence the temperature distribution through thick walled tubing is minimal; the fluid and tubing walls may be considered isothermal. It has previously been described that a primary advantage of using glass as a working material for  $\mu\text{TAS}$  applications is its low thermal conductivity [20]. However in the case of space-domain melting curve analysis a constant heat flux is required to heat the fluid throughout the analysis. The tubing walls/substrates act as an insulating layer between the heater blocks and the sample, resulting in a temperature disparity between the outer walls of the substrate and the actual fluid temperature.

The magnitude of this temperature disparity is proportional to the ramp rate seen by the fluid and to the thermal resistance between the fluid and the heater blocks. The ramp rate is a product of the spatial temperature gradient and the velocity of the fluid flow. It is clear from the results presented here that the temperature disparity is observable and will have an effect on denaturation temperature measurements. An equation has been presented which describes the temperature disparity for fluid in a simple tube and measure substrate thermal resistance. This approach can be applied to any micro-channel substrate to compensate for temperature disparity effects irrespective of knowledge of substrate dimensions or composition; with the caveats that the spatial temperature gradient applied to the walls of the substrate be

**Table 2**

Thermal resistance measurements made using melting analysis.

Method of	Equation	$R^2$	Thermal Res. ( $x/kA$ ) K/W
Substrate A	$y = 7.257x$	0.9270	7.396
Substrate B	$y = 5.151x$	0.9866	4.985

uniform and that the substrate be non-varying in the direction of heat flux.

It has also been shown that denaturation temperature measurements made at different velocities/spatial temperature gradients but at identical ramp rates are comparable. This approach has a number of advantages. In the case of an integrated  $\mu\text{TAS}$  system — where flow rates may be dictated by other factors — changing the spatial temperature gradient applied along the block allows the ramp rate to be selected. Decreasing the velocity of the fluid — and hence the time the sample is in the test rig — can result in a greater number of fluorescent  $acq/^\circ\text{C}$ . The number of fluorescent  $acq/^\circ\text{C}$  made by a high-resolution melting analysis platform is an important benchmark for its performance, particularly in SNP analysis [4]. In the work presented here melting curves measured at  $dT/dt = 0.033^\circ\text{C}$  across  $\Delta T = 24^\circ\text{C}$  resulted in approximately 100  $acq/^\circ\text{C}$ .

Of particular note were measurements made at  $dT/dt = 0.0^\circ\text{C}$ . In this case the velocity of the fluid was zero and the fluorescent acquisition system was traversed across the sample. Using this method it is clear that ramp rate effects are greatly attenuated. Unlike well-based systems [3] this approach will not require any compensation for thermal capacitance effects. In addition the number of fluorescent measurements made will be entirely a function of the viability of the test sample, resulting in the potential for very high-resolution melting analysis.

It is clear from this study that the effects of thermal resistance must be compensated for when trying to make cross-comparison of melting profiles acquired using space-domain melting analysis at different ramp rates; and indeed in different substrates/microchannel profiles. However this study describes a melting curve analysis based technique whereby the thermal resistance of substrates can be measured. This approach is non-invasive and can be applied to channel geometries where direct instrumentation — such as thermocouples — may not be possible. dsDNA can be used as an alternative to other on chip temperature sensing methods such as liquid crystal thermometry [34,23] and fluorescent dyes [35]. With denaturation temperatures ranging from  $\approx 60^\circ\text{C}$  to  $\approx 93^\circ\text{C}$  depending primarily on DNA strand length and composition; dsDNA has previously been used to measure temperatures in both well-based PCR systems [36] and also from substrate surfaces [19].

## References

- [1] C. Wittwer, N. Kuskawa, Molecular Microbiology: Diagnostic Principles and Practice, ASM Press, Washington DC, 2004, (Chapter 6) Real Time PCR.
- [2] C. Wittwer, M. Herrmann, A. Moss, R. Rasmussen, Continuous fluorescence monitoring of rapid cycle DNA amplification, Biotechniques 22 (1997) 130–138.
- [3] K. Ririe, R. Rasmussen, C. Wittwer, Product differentiation by analysis of DNA melting curves during the polymerase chain reaction, Analytical Biochemistry 245 (1997) 154–160.
- [4] M.G. Herrmann, J.D. Durtschi, L.K. Bromley, C.T. Wittwer, K.V. Voelkerding, Amplicon DNA melting analysis for mutation scanning and genotyping: cross-platform comparison of instruments and dyes, Clinical Chemistry 52 (3) (2006) 494–503.
- [5] C. Gundry, J. Vandersteen, G. Reed, R. Pryor, J. Chen, C. Wittwer, Amplicon melting analysis with labeled primers: a closed-tube method for differentiating homozygotes and heterozygotes, Clinical Chemistry 49 (3) (2003) 396–406.
- [6] P. Bernard, C. Wittwer, Real time PCR technology for cancer diagnostics, Clinical Chemistry 48 (2002) 1178–1185.

- [7] M. Hernandez, D. Rodriguez-Lazaro, T. Esteve, S. Prat, M. Pla, Development of melting temperature based SYBR Green I polymerase chain reaction methods for multiplex genetically modified organism detection, *Analytical Biochemistry* 323 (2003) 164–170.
- [8] A. Manz, N. Graber, H. Widmer, Miniaturized total chemical analysis systems: a novel concept for chemical sensing, *Sensors and Actuators B: Chemical* 1 (1990) 244–248.
- [9] H. Nagai, Y. Murakami, Y. Morita, K. Yokoyama, E. Tamiya, Development of a microchamber array for picoliter PCR, *Analytical Chemistry* 73 (2001) 1043–1047.
- [10] M. Kopp, A. de Mello, A. Manz, Chemical amplification: continuous-flow PCR on a chip, *Science* 280 (1998) 1046–1048.
- [11] I. Schneegass, J. Kohler, Flow-through polymerase chain reactions in chip thermocyclers, *Reviews in Molecular Biotechnology* 82 (2001) 101–121.
- [12] S.O. Sundberg, C.T. Wittwer, J. Greer, R.J. Prior, O. Elintoba-Johnson, B.K. Gale, Solution-phase DNA mutation scanning and SNP genotyping by nanoliter melting analysis, *Biomedical Microdevices* 9 (2) (2007) 159–166.
- [13] H. Mao, M.A. Holden, M. You, P.S. Cremer, Reusable platforms for high-throughput on-chip temperature gradient assays, *Analytical Chemistry* 71 (2002) 5071–5075.
- [14] T.M. Dalton, D.J. Kinahan, M.R. Davies, Fluorescent melting curve analysis compatible with a flowing polymerase chain reactor, in: *Proceedings of 2005 ASME International Mechanical Engineering Congress and Exposition*, ASME, 2005.
- [15] N. Crews, C. Wittwer, J. Montgomery, R. Pryor, B. Gale, Spatial DNA melting analysis for genotyping and variant scanning, *Analytical Chemistry* 81 (6) (2009) 2053–2058.
- [16] D.J. Kinahan, T.M. Dalton, M.R. Davies, ICNMM2008-62014 microchannel fluorescent melting curve analysis, in: *Proceedings of 2008 Sixth International Conference on Nanochannels, Microchannels and Minichannels*, ASME, 2008.
- [17] D.J. Kinahan, T.M. Dalton, M.R. Davies, Effect of substrate thermal resistance on space-domain microchannel fluorescent melting curve analysis, *Biomedical Microdevices* 11 (4) (2009) 747–754.
- [18] P. Baaske, S. Dühr, D. Braun, Melting curve analysis in a snapshot, *Applied Physics Letters* 91 (2007) 133901.
- [19] A. Dodge, G. Turcatti, I. Lawrence, N.F. de Rooij, E. Verpoorte, A microfluidic platform using molecular beacon-based temperature calibration for thermal dehybridization of surface-bound DNA, *Analytical Chemistry* 76 (6) (2004) 1778–1787.
- [20] B. Giordano, E. Copeland, J. Landers, Towards dynamic coating of glass microchip chambers for amplifying DNA via the polymerase chain reaction, *Electrophoresis* 22 (2) (2001) 334–340.
- [21] K. Sun, A. Yamaguchi, Y. Ishida, S. Matsuo, H. Misawa, A heater-integrated transparent microchannel chip for continuous-flow PCR, *Sensors and Actuators: B. Chemical* 84 (2–3) (2002) 283–289.
- [22] H. Zhang, D. Pinjala, T. Wong, K. Toh, Y. Joshi, Single-phase liquid cooled microchannel heat sink for electronic packages, *Applied Thermal Engineering* 25 (10) (2005) 1472–1487.
- [23] R. Muwanga, I. Hassan, Local heat transfer measurements in microchannels using liquid crystal thermography: methodology development and validation, *Journal of Heat Transfer* 128 (2006) 617.
- [24] D. Ross, M. Gaitan, L. Locascio, Temperature measurement in microfluidic systems using a temperature-dependent fluorescent dye, *Analytical Chemistry* 73 (17) (2001) 4117–4123.
- [25] D. Ross, L. Locascio, Microfluidic temperature gradient focusing, *Analytical Chemistry* 74 (11) (2002) 2556–2564.
- [26] R. Fu, B. Xu, D. Li, Study of the temperature field in microchannels of a PDMS chip with embedded local heater using temperature-dependent fluorescent dye, *International Journal of Thermal Sciences* 45 (9) (2006) 841–847.
- [27] M.N. Kashid, I. Gerlach, S. Goetz, J. Franzke, J.F. Acker, F. Platte, D.W. Agar, S. Turek, Internal circulation with the liquid slugs of a liquid-liquid slug-flow capillary microreactor, *Industrial and Engineering Chemistry Research* 44 (2005) 5003–5010.
- [28] P. Haugland, *Handbook of Fluorescent Probes and Research Products*, Molecular Probes, Oregon, 2002.
- [29] D.J. Kinahan, T.M. Dalton, M.R. Davies, ICNMM2008-62015 thermal resistance measurements from a microchannel fluorescent melting curve analysis platform, in: *Proceedings of the 2008 6th International Conference on Nanochannels, Microchannels and Minichannels*, ASME, 2008.
- [30] P. Holman, *Heat Transfer*, eighth ed. McGraw Hill International Editions, 1997.
- [31] A. Bejan, *Heat Transfer*, John Wiley and Sons, 1993.
- [32] M.B. Sayers, T.M. Dalton, M.R. Davies, Real-time fluorescence monitoring of the polymerase chain reaction in a novel continuous flow reactor for accurate DNA quantification, in: *Proceedings of 4th International Conference on Nanochannels, Microchannels and Minichannels*, ASME, 2006.
- [33] M. Chabert, K.D. Dorfman, P. de Cremoux, J. Roeraade, J.-L. Viovy, Automated microdroplet platform for sample manipulation and polymerase chain reaction, *Analytical Chemistry* 78 (2006) 7722–7728.
- [34] A. Chaudhari, T. Woudenberg, M. Albin, K. Goodson, Transient liquid crystal thermometry of microfabricated PCR vessel arrays, *Journal of Microelectromechanical Systems* 7 (4) (1998) 345–355.
- [35] J. Zhou, H. Yan, Y. Zheng, H. Wu, Highly fluorescent poly (dimethylsiloxane) for on-chip temperature measurements, *Advanced Functional Materials* 19 (2) (2009) 324–329.
- [36] C. Nellaker, U. Wallgren, H. Karlsson, Molecular beacon-based temperature control and automated analyses for improved resolution of melting temperature analysis using SYBR I green chemistry, *Clinical Chemistry* 53 (1) (2007) 98.